Journal of Alloys and Compounds 560 (2013) 142–146

Contents lists available at SciVerse ScienceDirect

Journal of Alloys and Compounds

journal homepage: www.elsevier.com/locate/jalcom

Biotemplating fabrication, mechanical and electrical characterizations of NbC nanowire arrays from the bamboo substrate

Jun Du [a], Yingchao Yang [b], Zheng Fan [c], Yang Xia [a], Xuejuan Cheng [a], Yongping Gan [a], Hui Hang [a], Lixin Dong [c], Xiaodong Li [b], Wenkui Zhang [a,*], Xinyong Tao [a,*]

[a] College of Chemical Engineering and Materials Science, Zhejiang University of Technology, Hangzhou 310014, PR China
[b] Department of Mechanical Engineering, University of South Carolina, 300 Main Street, Columbia, SC 29208, USA
[c] Department of Electrical and Computer Engineering, Michigan State University, East Lansing, MI 48824, USA

ARTICLE INFO

Article history:
Received 16 January 2013
Received in revised form 1 February 2013
Accepted 4 February 2013
Available online 13 February 2013

Keywords:
NbC
Biotemplate method
Young's modulus
Electrical property

ABSTRACT

In this work, NbC nanowire arrays were successfully synthesized via a facile and cost-effective biotemplate method. Natural bamboo chips were used as both the carbon source and the template for formation of catalyst particles, which significantly simplify the synthesis process of NbC nanowire arrays. Based on the structural, morphological, and elemental analyses, a fluoride-assisted vapor–liquid–solid growth mechanism was proposed. *In situ* nanoscale three-point bending measurements demonstrated that the Young's modulus of NbC nanowires was in the range from 281 to 453 GPa with an average value of 338 ± 55 GPa. The resistivity of NbC nanowires was further investigated by *in situ* electrical property characterization using a multipoint measurement inside a transmission electron microscope. The resistivity of NbC nanowires was calculated to be 5.02 mΩ cm.

1. Introduction

Transition metal carbides (TMCs) have been studied extensively as high-temperature-resistant composites [1], coatings [2], cutting tools [3], superconducting devices [4], energy storage electrodes [5], and catalysts [2,6,7], due to their elevated melting points, excellent mechanical properties, high resistance to oxidizing acids, and good electrical and thermal conductivities. NbC, as one of TMC, is known to possess a unique combination of valuable properties. It exhibits a high toughness (3–6 MPa $m^{1/2}$), high hardness (20–22 GPa), high melting point (3873 K) and Young's modulus (400–500 GPa) [8,9], excellent chemical stability, together with superior wear resistance. It has been used as wear resistant [10], medical [11] and chemical materials [12].

In the past decades, one-dimensional (1D) TMC nanostructures such as nanowires [13] and nanorods [14] have drawn extensive attention because of their size-dependent optical, electronic [13–15], mechanical [13,14,16], and field emission properties [17], opening up unprecedented opportunities for constructing nano-devices with new functionalities. However, there are only few routes for synthesizing 1D NbC nanostructures. Moreover, 1D NbC nanostructures' mechanical and electrical properties are still lacking in literature. This limits their applications in constructing NbC based nanocomposites and nano-devices. To date, various techniques including carbon nanotube confined reaction [18], chemical vapor deposition [19], carbon thermal reduction [20–22], and pyrolysis of polymeric precursors [23] have been developed for the preparation of 1D carbide nanostructures. In our recent studies, a facile and cost-effective biotemplating method has been developed to synthesize 1D TMC nanostructures [13,14,24].

In this paper, we demonstrate, for the first time, that NbC nanowire arrays can be fabricated by a facile biotemplate method. Using *in situ* atomic force microscopy (AFM) and transmission electron microscopy (TEM), the Young's modulus and the resistivity of individual NbC nanowires were measured, providing critical parameters for practical applications.

2. Experimental section

Dried bamboo chips (wide: 2.5 mm; length: 0.7 mm; thickness: 0.2 mm) were immersed in ethanol solution of acetone with 0.2 mol/L concentration. After stirring for 0.5 h, bamboo chips were dried at 80 °C for 30 min, then at 110 °C for 2 h in an oven. 0.375 g of NaF, 2.372 g of Nb_2O_5 and 0.259 g of $Ni(NO_3)_2$ $6H_2O$ were dissolved into 20 ml ethanol to form a Nb–Ni–F emulsion under ultrasound irradiation. Bamboo chips were dipped in the Nb––Ni–F emulsion. After stirring for 2 h, the bamboo chips were dried at 90 °C for 30 min in a preheated oven and finally cured at 110 °C for 1 h. The bamboo substrates were then inserted into a sealed graphite crucible and then heated to 1250 °C at a heating rate of 5 °C/min and maintained at that temperature for 1 h under a constant Ar gas flow (350 sccm). After deposition, the furnace was cooled to room temperature.

* Corresponding authors. Tel.: +86 571 88320394 (W. Zhang).
E-mail addresses: ldong@egr.msu.edu (L. Dong), lixiao@cec.sc.edu (X. Li), msechem@zjut.edu.cn (W. Zhang), tao@zjut.edu.cn (X. Tao).

0925-8388/$ - see front matter © 2013 Elsevier B.V. All rights reserved.
http://dx.doi.org/10.1016/j.jallcom.2013.02.005

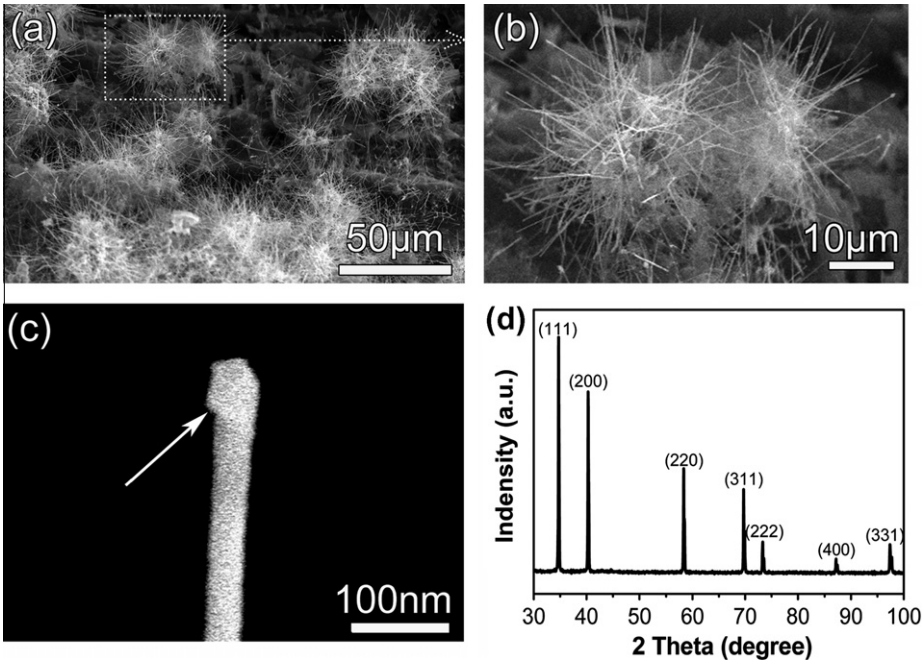

Fig. 1. (a) SEM image of NbC nanowire arrays on the bamboo substrate; (b) partial enlargement SEM image in (a); and (c) an individual NbC nanowire. (d) XRD pattern of NbC nanowire arrays.

The phase of the as-prepared products was determined by X-ray diffraction (XRD) using an XPert Pro diffractometer with a step size of 0.02 for Cu Kα radiation (λ = 1.5418 Å). Scanning electron microscopy (SEM, Hitachi s-4800) and transmission electron microscope (TEM,FEI Tecnai G2 F30) equipped with an energy-dispersive X-ray spectroscopy (EDS) detector were applied to investigate the microstructure and morphology. A drop of an ethanol solution containing the nanowires was placed on a stan dard atomic force microscope (AFM) reference sample (Veeco Metrology Group) with uniform trenches. In order to avoid nanowire sliding during the bending tests, both ends of the nanowire, which bridged the trench, were clamped by 20 min electron beam-induced deposition (EBID). A Veeco Dimension 3100 AFM was used to perform three-point bending tests by directly indenting the center of a suspended nanowire that bridged the channel with a tapping-mode silicon AFM tip. A total of 15 bending tests were performed to obtain the Young's modulus. The electrical properties of individual nanowires are characterized using a scanning tunneling microscope–transmission electron microscope (STM–TEM) holder (FM2000E, Nanofactory Instruments AB) in a TEM (JEOL 2200FS) with a field emission gun.

3. Results and discussion

The morphologies of the as-prepared products were characterized by SEM. Fig. 1a is the low magnification SEM image of nanowire arrays. The image clearly reveals that an abundance of uniform and straight nanowire arrays grew on the bamboo substrate. The magnified image (Fig. 1b) shows that nanowires have a length of 1–50 μm and a diameter of 30–100 nm. As indicated by the arrow in Fig. 1c, there is a quasi-spherical-shaped catalyst particle at the tip of the nanowire, indicating the top growth mechanism of this nanowire. The XRD pattern of the prepared NbC nanowire arrays is shown in Fig. 1d, in which seven diffraction peaks could be distinguished. The reflections at 34.7°, 40.2°, 58.3°, 69.7°, 73.3°, 87.1° and 97.3° are indexed to the diffractions from the (1 1 1), (2 0 0), (2 2 0), (3 1 1), (2 2 2), (4 0 0), and (3 3 1) crystal family planes of cubic NbC (JCPDS 65-0281). No Nb_xO_y, NbO_xC_y and Nb can be detected, suggesting that Nb_2O_5 was successfully converted to NbC.

Further structural characterization using transmission electron microscopy (TEM) is depicted in Fig. 2. Fig. 2a shows a low magnification, bright-field image of an individual nanowire with the growth direction along [0 1 0] of cubic NbC nanowire. It reveals that the diameter of the nanowire is less than 100 nm. The TEM results are in accordance with the SEM observations as shown in Fig. 1. As indicated by the black arrow in Fig. 2a, there is a catalyst particle at the tip of the nanowire, indicating a VLS growth mechanism [25] for the NbC nanowire. The EDS spectrum reveals that the catalyst particle contains C, Nb, and Ni. Fig. 2b shows the HRTEM image taken from the nanowire (as indicated by the red[1] arrow in Fig. 2a). The space between two adjacent lattice fringes is 0.22 nm, corresponding well to the {0 1 0} planes of NbC. Fig. 2c shows the corresponding indexed fast Fourier transform (FFT) pattern of the NbC nanowire in Fig. 2b, indicating that the NbC NW is a single crystal with the growth direction along [0 1 0].

During the VLS growth of NbC nanowires, there must be gas-phase transport of C and Nb to the Ni catalyst particle. In this work, bamboo chips acted as the renewable carbon source. Fig. 3 shows the decomposition product of bamboo cellulose at high temperature. On one hand, during pyrolysis (Eq. (1)), bamboo cellulose undergoes: (1) condensable vapors were condensed into a liquid product (tar), (2) condensable gases, and (3) solid carbon that consists of elemental carbon [26]. On the other hand, cracking of tars (Eq. (2)) occurred under high-temperature calcination (1250 °C), which is believed to be a significant pathway for production of CO, H_2, and several light hydrocarbon gases such as CH_4, C_2H_2, C_2H_6, and C_3H_6 [27]. These hydrocarbon gases resulting from pyrolysis of cellulose served as the carbon source

$$(C_6H_{10}O_5)_n \rightarrow C_3H_6(g) + C_2H_6(g) + C_2H_2(g) + CH_4(g) + CO_2(g) + CO(g) + H_2O(g) + H_2(g) + \text{tars(l)} + \text{char(s)} \quad (1)$$

$$\text{tars} \rightarrow C_xH_y(g) + C_2H_5OH(g) + CH_4(g) + CH_3OH(g) + CH_3CHO(g) + CH_2O(g) + H_2O(g) + H_2(g) + CO_2(g) + CO(g) \quad (2)$$

[1] For interpretation of color in 'Fig. 2', the reader is referred to the web version of this article.

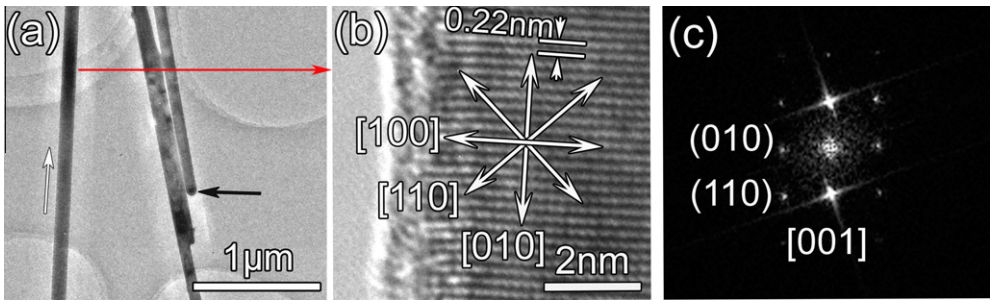

Fig. 2. (a) TEM image of a NbC nanowire. (b) The [001] zone axis HRTEM image of the NW in (a). (c) The corresponding FFT diffraction pattern obtained from (b).

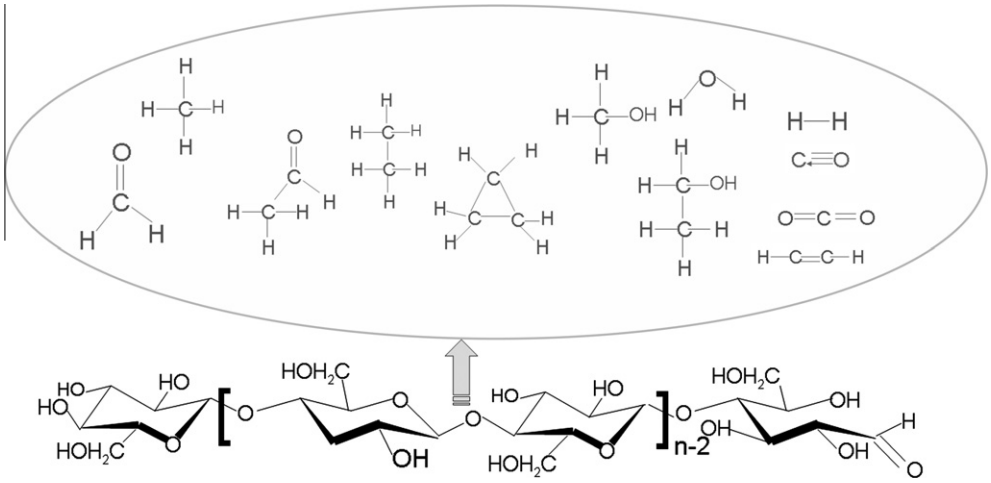

Fig. 3. Decomposition schematics of bamboo cellulose.

It was found that NaF played a critical role in growth of nanowires. No NbC nanowire array was obtained without introducing fluorides. Gaseous fluoride species and such as $NbOF_2(g)$, $NbF_4(g)$, and $NbF_3(g)$ can be formed at the reaction temperature and must be responsible for the transport of Nb. The following reactions are expected to occur during growth of NbC nanowires

$$Nb_xF_y(g) + Ni(l) + C(g) \rightarrow yF(g) + Ni(Nb,C)(l) \quad (3)$$

$$Ni(Nb,C)(l) \rightarrow NbC(s) + Ni(l) \quad (4)$$

Based on these results, we propose a fluoride-assisted vapor–liquid–solid (VLS) growth mechanism (Fig. 4). During the VLS growth of NbC nanowire, all reactions are not consecutive but probably occur simultaneously. On one hand, Ni catalyst nanoparticles can be produced on surface of the bamboo substrate during calcinations, which can absorb C and Nb source gases (Eq. (3)). On the other hand, when the catalyst droplet Ni(Nb,C) supersaturates with Nb and C, NbC nanowire may precipitate and grow up via a top growth mechanism (Eq. (4)).

To investigate the mechanical properties of NbC nanowires, *in situ* AFM three-point bending tests were performed directly on individual nanowires to obtain the elastic modulus (Fig. 5a). To avoid sliding during bending tests, both ends of the nanowires, which bridged the trench, were fixed with EBID of carbon. Fig. 5b and c are the SEM and AFM images of an EBID-fixed nanowire, respectively. Fig. 5d shows representative force–piezo position (*F–Z*) curves for a NbC nanowire on substrate (for calibration) and a suspended NbC nanowire arrays. The *F–Z* curves exhibit a strong linear relationship up to 900 nN. Under the premise of the assumption that the nanowires follows the linear elastic theory

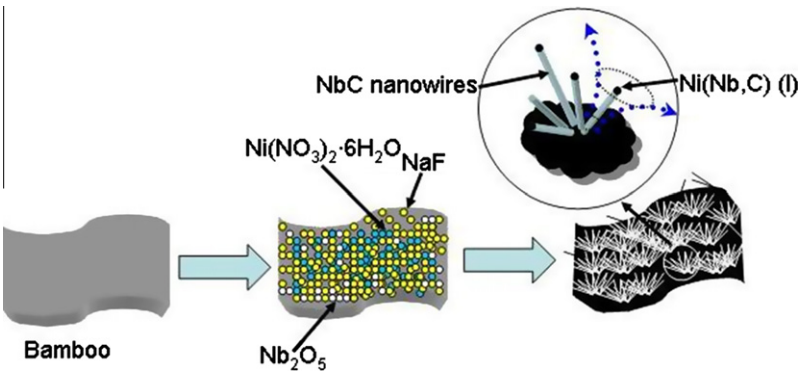

Fig. 4. Schematics image demonstrating the formation mechanism of NbC nanowire arrays.

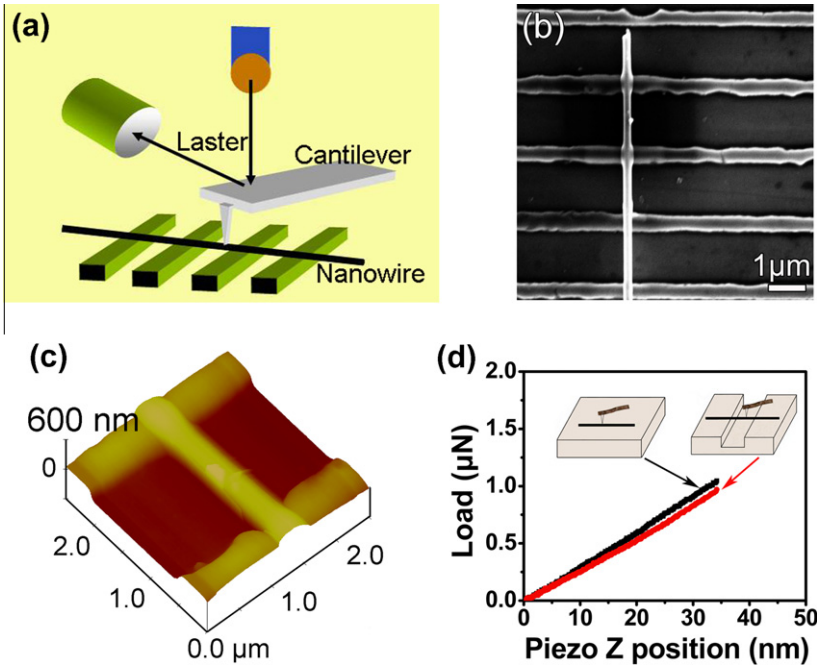

Fig. 5. (a) Schematic diagram of AFM *in situ* mechanical properties of a single nanowire. (b) SEM image of EBID-fixed nanowires. (c) 3D AFM image of the corresponding nanowire. (d) Representative bending *F–Z* curves for the nanowire on substrate (for calibration) and the suspended nanowire.

of an isotropic material, the elastic modulus of the nanowires, En, can be calculated from [28]

$$\mathrm{En} = (\mathrm{KnL}^3)/(192\mathrm{I}) \tag{5}$$

$$\mathrm{Kn} = K_1K_2/(K_1 - K_2) \tag{6}$$

where L is the suspended length of the nanowire and I is the moment of inertia. K_1 and K_2 are the slopes of the curves from the nanowire on substrate (for calibration) and the suspended nanowire, respectively. The measured Young's modulus of NbC nanowires is in the range from 281 to 453 GPa with an average value of 338 ± 55 GPa, which is close to the spark plasma sintered NbC powers(296–330 GPa) [8,9], but lower than the theoretically predicted value of 484 GPa . This decrease in Young's modulus may result from the high surface-to-volume ratio (surface effect) of nanowires. Similar phenomena have been reported for other nanowires such as borates and silicon [29,30].

Fig. 6 shows the *in situ* characterization of individual NbC nanowires in TEM. A multipoint technique [13] (Fig. 6a) was used for the *in situ* electrical property characterization of individual nanostructures inside TEM with a nanomanipulator. Fig. 6b shows the equivalent circuit of this technique, where $R_{\mathrm{NW\text{-}P}}$, R_{NW}, $R_{\mathrm{S\text{-}NW}}$, and R_{S} represent the contact resistance of the probe to the nanostructure, the resistance of the nanostructure, the contact resistance of the sample holder to the nanostructure, and the resistance of the sample holder, respectively. The resistance of the sample can be calculated by $R_{\mathrm{NW}} = R_{\mathrm{NW\text{–}TIP}} - R_{\mathrm{NW\text{-}ROOT}} = (R_{\mathrm{S}} + R_{\mathrm{S\text{-}NW}} + R_{\mathrm{NW\text{-}P}} + R_{\mathrm{NW\text{–}TIP}}) - (R_{\mathrm{S}} + R_{\mathrm{S\text{-}NW}} + R_{\mathrm{NW\text{-}P}} + R_{\mathrm{NW\text{-}ROOT}})$ [13]. Fig. 6c shows IV curves of an individual NbC nanowire obtained by contacting the probe to the tip (inset: left) or the root (inset: right) of an individual NbC, respectively. The resistivity of the nanowire at 500 mV was calculated to be 5.02 mΩ cm. Based on the remarkable mechanical and electrical properties, this kind of NbC arrays shows promising applications in field emission, catalysis, nano-devices, nanocomposites, etc.

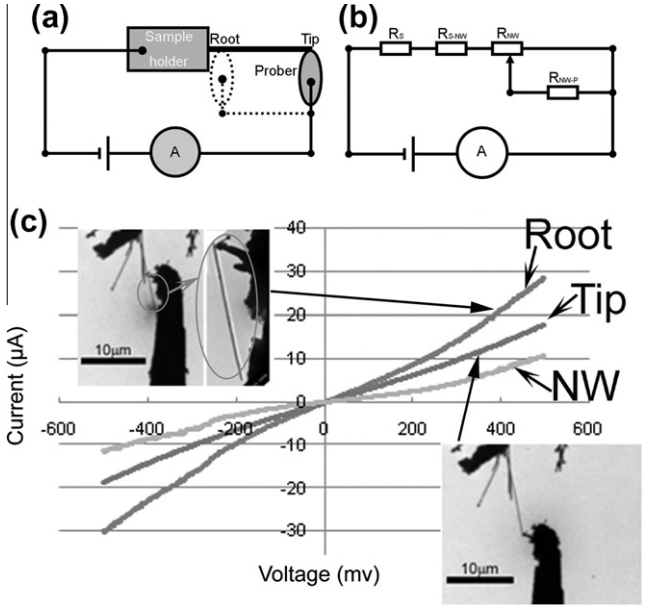

Fig. 6. *In situ* TEM multipoint measurement tests. (a) Schematic of multipoint technique for *in situ* electric property characterization. By contacting a probe to different points on an individual nanostructure, the resistance of nanostructures is measured. (b) The equivalent circuit of this technique. (c) The IV characterization of individual NbC NWs. The insets are corresponding TEM images.

4. Conclusion

We have demonstrated a simple approach to prepare NbC nanowire arrays via biotemplate method. The growth of the nanowire arrays is attributed to a VLS mechanism. Mechanical behavior of individual NbC nanowires has been probed by *in situ* AFM method. The measured Young's modulus of NbC nanowires is in the range from 281 to 453 GPa, which is close to the spark plasma sintered NbC powers(296–330 GPa), but lower than the theoretically

predicted value of 484 GPa. *In situ* TEM probe multipoint tests revealed that the electrical resistivity of the NbC nanowire was about 5.02 mΩ cm.

Acknowledgments

This work is financially supported by the NSFC (51002238 and 51172205), Zhejiang Provincial NSF of China (Y4090420), Qianjiang Talent Project (2010R10029), 'Qianjiang Scholars' program, and project sponsored by the Project-sponsored by SRF FOR ROCS (2010609), State Education Ministry. X.D.L and Y.C.Y acknowledge funding by NSF (CMMI-1129979 and CMMI-0968843).

References

[1] B.V.M. Kumar, B. Basu, Int. J. Refract. Met. H 26 (2008) 504–513.
[2] G. Dong, B.A. Yan, Q.L. Deng, T. Yu, J. Wuhan Univ. Technol. 27 (2012) 231–237.
[3] B. Zou, C.Z. Huang, J.P. Song, Z.Y. Liu, L. Liu, Y. Zhao, Int. J. Refract. Met. H 35 (2012) 1–9.
[4] W.S. Williams, Jom-J. Min. Met. Mat. S 50 (1998) 62–66.
[5] Y. Gao, V. Presser, L.F. Zhang, J.J. Niu, J.K. McDonough, C.R. Perez, H.B. Lin, H. Fong, Y. Gogotsi, J. Power Sources 201 (2012) 368–375.
[6] R. Radis, E. Kozeschnik, Modell. Simul. Mater. Sci. 20 (2012).
[7] Y. Kitaura, Y. Kaneno, T. Takasugi, Mater. Sci. Eng. A-Struct. 527 (2010) 6012–6019.
[8] P. Soni, G. Pagare, S.P. Sanyal, M. Rajagopalan, J. Phys. Chem. Solids 73 (2012) 873–880.
[9] P. Soni, G. Pagare, S.P. Sanyal, J. Phys. Chem. Solids 72 (2011) 810–816.
[10] Y.Y. Xia, M.W. Zhao, X.D. Liu, C. Song, T. He, J.X. Fang, AIP. Adv. 2 (2012).
[11] M. Braic, V. Braic, M. Balaceanu, A. Vladescu, C.N. Zoita, I. Titorencu, V. Jinga, F. Miculescu, Thin Solid Films 519 (2011) 4064–4068.
[12] Z. Xiong, G.Q. Shao, X.L. Shi, X.L. Duan, P. Sun, T.G. Wang, Mater. Lett. 61 (2007) 3071–3074.
[13] X.Y. Tao, J. Du, Y.P. Li, Y.C. Yang, Z. Fan, Y.P. Gan, H. Huang, W.K. Zhang, L.X. Dong, X.D. Li, Adv. Energy Mater. 1 (2011) 534–539.
[14] X.Y. Tao, J. Du, Y.C. Yang, Y.P. Li, Y. Xia, Y.P. Gan, H. Huang, W.K. Zhang, X.D. Li, Cryst. Growth Des. 11 (2011) 4422–4426.
[15] J. Lussien, D. Morvan, J. Amouroux, D. Rousselle, E. Bruneton, F. Blein, Prog. Plasma Process. Mater. 2001 (2001) 623–632.
[16] J. Kano, N. Solihin, S. Sato, F. Suzuki, H. Saito, T. Suginobe, ISIJ Int. 49 (2009) 458–462.
[17] X.M. Zhang, K.F. Huo, H.R. Wang, B.A. Gao, J.J. Fu, T.F. Hung, P.K. Chu, ACS Appl. Mater. Int. 4 (2012) 1037–1042.
[18] N.B. Dahotre, P. Kadolkar, S. Shah, Surf. Interface Anal. 31 (2001) 659–672.
[19] M. Lei, K. Huang, R. Zhang, H.J. Yang, X.L. Fu, Y.G. Wang, W.H. Tang, J. Alloys Comp. 535 (2012) 50–52.
[20] H. Zuhailawati, H.M. Salihin, Y. Mahani, J. Alloy. Comp. 489 (2010) 369–374.
[21] N. Nedfors, O. Tengstrand, E. Lewin, A. Furlan, P. Eklund, L. Hultman, U. Jansson, Surf. Coat. Technol. 206 (2011) 354–359.
[22] F.A.O. Fontes, J.F. de Sousa, C.P. Souza, M. Benachour, M.B.D. Bezerra, Chem. Eng. J. 184 (2012) 303–307.
[23] C.S. Sharma, H. Katepalli, A. Sharma, M. Madou, Carbon 49 (2011) 1727–1732.
[24] X.Y. Tao, Y.P. Li, J. Du, Y. Xia, Y.C. Yang, H. Huang, Y.P. Gan, W.K. Zhang, X.D. Li, J. Mater. Chem. 21 (2011) 9095–9102.
[25] Y.N. Xia, P.D. Yang, Y.G. Sun, Y.Y. Wu, B. Mayers, B. Gates, Y.D. Yin, F. Kim, Y.Q. Yan, Adv. Mater. 15 (2003) 353–389.
[26] J.M. Cho, J.M. Davis, G.W. Huber, Chem. Sus. Chem. 3 (2010) 1162–1165.
[27] M. Zhao, N.H. Florin, A.T. Harris, Appl. Catal. B-Environ. 97 (2010) 142–150.
[28] X.Y. Tao, L.X. Dong, X.N. Wang, W.K. Zhang, B.J. Nelson, X.D. Li, Adv. Mater. 22 (2010) 2055–2059.
[29] X.Y. Tao, X.D. Li, Nano Lett. 8 (2008) 505–510.
[30] Y. Zhu, F. Xu, Q.Q. Qin, W.Y. Fung, W. Lu, Nano Lett. 9 (2009) 3934–3939.